Charged Local Anesthetics Block Ionic Conduction in the Sheep Cardiac Sarcoplasmic Reticulum Calcium Release Channel

Andrew Tinker and Alan J. Williams
Department of Cardiac Medicine, National Heart and Lung Institute, University of London, London, SW3 6LY, England

ABSTRACT We have examined the effect of the charged local anesthetics QX314, QX222, and Procaine on monovalent cation conduction in the Ca^{2+} release channel of the sheep cardiac sarcoplasmic reticulum. All three blockers only affect cation conductance when present at the cytoplasmic face of the channel. QX222 and Procaine act as voltage-dependent blockers. With 500 Hz filtering, this is manifest as a relatively smooth reduction in single-channel current amplitude most prominent at positive holding potentials. Quantitative analysis gives an effective valence of approximately 0.9 for both ions and $K_b(0)$s of 9.2 and 15.8 mM for QX222 and Procaine, respectively. Analysis of the concentration dependence of block suggests that QX222 is binding to a single site with a K_m of 491 μM at a holding potential of 60 mV. The use of amplitude distribution analysis, with the data filtered at 1 to 2 kHz, reveals that the voltage and concentration dependence of QX222 block occurs largely because of changes in the blocker on rate. The addition of QX314 has a different effect, leading to the production of a substate with an amplitude of approximately one-third that of the control. The substate's occurrence is dependent on holding potential and QX314 concentration. Quantitative analysis reveals that the effect is highly voltage dependent, with a valence of approximately 1.5 caused by approximately equal changes in the on and off rates. Kinetic analysis of the concentration dependence of the substate occurrence reveals positive cooperativity with at least two QX314s binding to the conduction pathway, and this is largely accounted for by changes in the on rate. A paradoxical increase in the off rate at high positive holding potentials and with increasing QX314 concentration at 80 mV suggests the existence of a further QX314-dependent reaction that is both voltage and concentration dependent. The substate block is interpreted physically as a form of partial occlusion in the vestibule of the conduction pathway giving a reduction in single-channel current by electrostatic means.

INTRODUCTION

Release of Ca^{2+} from the sarcoplasmic reticulum (SR) is thought to be a critical factor in the chain of events initiating contraction in cardiac and skeletal muscle (1–3). In both muscle types Ca^{2+} is released through ligand-regulated ion channels localized in specialized regions where the SR membrane network forms junctions with the sarcolemma (4). The properties of both skeletal and cardiac SR Ca^{2+}-release pathways have been investigated at the single-channel level under voltage clamp conditions following the incorporation of isolated junctional SR membrane vesicles into planar phospholipid bilayers (5–7), and such studies have provided considerable information concerning the regulation of channel gating by physiological (5, 8, 9) and pharmacological (10) agents.

Detailed investigations of the mechanisms governing ion conduction in the SR Ca^{2+} release channel cannot be undertaken following the incorporation of isolated, intact, SR membrane vesicles into planar phospholipid bilayers due to the coincorporation of the monovalent cation and anion channels of this membrane. However, such studies are feasible following the purification of the Ca^{2+} release channel protein from the SR membrane. The demonstration of a specific, high-affinity interaction between the Ca^{2+} release channel of the SR and the plant alkaloid ryanodine has provided the impetus for the development of protocols for the purification of the ryanodine receptor and its identification as the Ca^{2+} release channel protein (11–13). We have purified the ryanodine receptor from sheep cardiac muscle SR, and following reconstitution, this protein complex functions as a ligand-sensitive, cation-selective channel (14). Using this preparation we have carried out a detailed characterization of the mechanisms of ion conduction, discrimination, and block in this channel (15–19).

In skinned skeletal muscle fibers contraction and release of Ca^{2+} from the SR is inhibited by the addition of Procaine and tetracaine (20). In addition, the release of Ca^{2+} from isolated canine cardiac SR vesicles can be inhibited by a wide range of hydrophobic compounds including two local anesthetics, Procaine and SKF 525-A (21, 22). Local anesthetics and related drugs are known to inhibit Na^+ channel current by interacting with the channel conduction pathway to block the passage of permeant ions (chapter 12 in Ref. 23). These observations have prompted us to examine the actions of three charged local anesthetics, Procaine, QX222, and QX314 on monovalent cation flux in the purified sheep cardiac SR Ca^{2+} release channel. The use of these cations makes interpretation of experimental data easier in that they are more than 95% charged at pH 7.4, and as a result only small quantities will partition into and cross lipid bilayers (24). The data reported here demonstrate block of monovalent cation current in the SR Ca^{2+} release channel by these charged local anesthetics.

MATERIALS AND METHODS

Materials

Phosphatidylethanolamine was purchased from Avanti Polar Lipids (Birmingham, AL), and phosphatidylcholine was from Sigma, Ltd.

Received for publication 29 January 1993 and in final form 30 March 1993.
Address reprint requests to Dr. Alan Williams.

0006-3495/93/08/852/13 $2.00

(Poole, Dorset, England). [^{3}H]Ryanodine was obtained from New England Nuclear (Boston, MA). Aqueous counting scintillant was purchased from Packard (Groningen, the Netherlands). The chloride salts of QX222 and QX314 were kind gifts from Astra Pharmaceuticals, Ltd. (Kings Langley, Hertfordshire, England). Procaine chloride was obtained from Sigma. The chemical structures of these compounds are shown in Hille (Ref. 23, p. 286). These ions were dissolved in the standard experimental 210 mM K^+ solution to make concentrated stock solutions from which small aliquots were added to the solutions in the *cis* and *trans* chambers. Other chemicals used were obtained as best available grade from BDH, Ltd. (Dagenham, Essex, England), Aldrich Chemical Company (Gillingham, Dorset, England), or Sigma.

Preparation of the purified sheep cardiac SR Ca^{2+} release channel

The biochemical isolation of the purified sheep cardiac Ca^{2+} release channel was carried out as previously described (14).

Planar lipid bilayer methods

Lipid bilayers, formed from suspensions of phosphatidylethanolamine in *n*-decane (35 mg/ml), were painted across a 200-μm diameter hole in a polystyrene copolymer partition that separated two chambers referred to as the *cis* (volume 0.5 ml) and *trans* (volume 1.5 ml) chambers. The *trans* chamber was held at virtual ground, and the *cis* chamber could be clamped at various holding potentials relative to ground. Current flow across the bilayer was measured with an operational amplifier as a current-voltage converter as described by Miller (25). Bilayers were formed in solutions of 200 mM KCl and 20 mM 4-(2-hydroxyethyl)-1-piperazineethanesulfonic acid and titrated with KOH to pH 7.4, resulting in a solution containing 210 mM K^+. An osmotic gradient was established by the addition of a small quantity (usually 50 to 100 μl) of 3 M KCl to the *cis* chamber. Proteoliposomes were added to the *cis* chamber and stirred. To induce fusion of the vesicles with the bilayer a second small aliquot (50 to 100 μl) of 3 M KCl was added to the *cis* chamber. After channel incorporation, further fusion was prevented by perfusion of the *cis* chamber with 210 mM K^+. Solutions contained 10 μM contaminant free Ca^{2+}, which was generally sufficient for channel activation. Very occasionally it was necessary to raise the Ca^{2+} in the *cis* chamber to 100 μM to obtain sufficient activation. Experiments were carried out at room temperature (21 $\pm$ 2°C).

The receptor channel incorporates in a fixed orientation in the bilayer; the *cis* chamber corresponds to the cytosolic face of the channel and the *trans* to the luminal (14, 16). In the subsequent discussion this naming convention will be adopted, and current flowing from the cytoplasm to the interior of the SR will be referred to as positive ground.

Single-channel data acquisition

Single-channel current fluctuations were displayed on an oscilloscope and stored on videotape. For analysis, data were replayed, filtered with an eight-pole Bessel filter, and digitized using an AT-based computer system (Satori, Intracel, Cambridge, England). Single-channel current amplitudes, amplitude histograms, and dwell time histograms were determined from digitized data. The representative traces shown in the figures were displayed on a Hewlett-Packard 7475A plotter following digitization with a PDP 11/73-based system (Indec, Sunnyvale, CA).

Methods of analysis

Calculation of blocking parameters

Single-channel current amplitudes were measured with manually controlled screen cursors to mark the open and closed levels. The data were filtered at 500 Hz and digitized at 2 kHz.

The blocking parameters given in the text for QX222 and Procaine are calculated from nonlinear regression fits of the Woodhull equation (26) (Eq. 1 in Results) of mean relative conductance to holding potential using a commercially available program (Graphpad Inplot v 4.03; GraphPad Software, San Diego, CA). The nonlinear regression program generates SEMs. However, these figures should be treated cautiously as only approximate measures of data spread. Such an approach has the possible theoretical advantage over linearization of the data, and subsequent use of linear regression that points at negative holding potentials, where there may only be a small reduction in relative conductance from 1.0, are not exaggerated in their importance in determining the effective valence of block. However, in practice the method used made only a small difference to the results obtained. For example, when the block induced by 2 mM QX222 (n = 7) using the above approach, the effective valence of block is 0.91 and the $K_b(0)$ is 9.2 mM. From the linearization of the data, values of 0.83 and 9.4 mM, respectively, are obtained. Alternatively, if each experiment is subjected to the Woodhull analysis, and mean effective valencies and $K_b(0)$ are calculated on that basis, then the figures obtained are, using nonlinear regression 0.93 and 11.1 mM respectively, and using the linearized plot 0.83 and 9.1 mM, respectively. The differences between these values are not large.

Using amplitude distribution analysis to estimate blocker kinetics

The beta function, as described by Fitzhugh (27), Yellen (28), and Quayle et al. (29), was used to estimate the kinetics of QX222 interaction with the receptor channel. Data were filtered at 1–2 kHz and digitized at 8 kHz. Amplitude histograms were compiled from parts of single-channel recording where the receptor channel was mostly open. Only a single channel was apparently active in such runs. Generally such histograms consisted of at least 2000 and often more digitized points, the great majority of which corresponded to open channel noise and a smaller proportion to baseline noise. The amplitude bin size for data acquisition was 1 pA. In addition, patches of data were selected where no channel activity was apparent, and amplitude histograms were compiled. These histograms were fitted with a simple gaussian which yielded a SD for the baseline noise. With 2 kHz filtering this was generally 1–2 pA. A personal computer-executable computer program was written that fit a generated probability density function for a two-state blocking-unblocking process with first-order filtering (see Eq. 3 in Results) convolved with noise to the experimental amplitude distribution. The outline of the approach is as follows:

1. The amplitude histogram, SD of the baseline noise, and control current amplitude under a given set of experimental conditions are retrieved.
2. The amplitude histogram is standardized by dividing by the control current.
3. A composite probability density function is generated corresponding to (*a*) the baseline noise, described by a factored gaussian distribution with the given noise standard deviation, and (*b*) the open channel noise, described by an appropriately scaled β function (Eq. 3 in Results) convolved with a gaussian noise distribution with a SD equal to that determined for the baseline. Standard numerical approximations are available for the gaussian, β, and γ functions (30).
4. The closeness of fit of the composite and scaled probability density function to the standardized amplitude histogram is then assessed by calculating the squared difference between the data points and the theoretical curve.
5. The three free variables (the number of events due to baseline noise, a and b) are then varied until a mininimum squared difference between the data points and the theoretical curve is found. This search is performed using a simplex algorithm (30).
6. The best fit theoretical curve and the amplitude histogram are downloaded to a graphics package to visually check the fit and to generate hardcopy.

The program converges to the same values, even given quite disparate guesses. The values for the kinetic parameters agree within 5% if obtained from a series of different amplitude histograms compiled from a run of data under given experimental conditions. K_{on} and K_{off} can then be determined from b and a using the approximation for an eight-pole Bessel filter and the filtering frequency (28). Yellen notes that the correspondence between theory and the approximation is good if $a, b > 2$. We have also adjusted the

filtering to ensure this, and 2 kHz was generally adequate. On occasions it was necessary to filter at the lower frequencies of 1 and 1.5 kHz.

Determining kinetics for block by QX314

The addition of QX314 leads to the production of a reduced conductance level associated with the normal fully open current amplitude in a manner qualitatively similar to that described previously for tetrabutyl and tetrapentyl ammonium (17).

In such records two measurements of current amplitude were made. The first is a measurement of the full conductance event (i.e., the current amplitude between the baseline and dotted line in the lower right-hand trace in Fig. 7*a*). The other is a measurement of the reduced conductance event (i.e., between the baseline and the level indicated by the arrow in the lower right-hand trace in Fig. 7*a*).

From runs of such data, where only an apparently single active channel is present, it is possible to determine kinetic parameters. The data were filtered at 4 kHz and digitized at 10 kHz. Open, substate and closed lifetime files were compiled using a 50% amplitude detection threshold with the cursors set manually on the fully open level (dotted line in the lower right-hand trace in Fig. 7*a*), the substate level (arrowed in the lower right-hand trace in Fig. 7*a*), and the closed level (baseline in the lower right-hand trace in Fig. 7*a*). Events above the midpoint between the open and substate level were considered to be open events, those below this but above the midpoint between the substate and closed level were considered to be substate events, and those below the latter midpoint were taken as closed events. Using this approach it was possible to obtain the total time spent in each state and dwell time histograms for each corresponding state. In cases where the openings rarely reached the fully open level (at high positive holding potentials and high QX314 concentrations) the cursor was placed at a level comparable to the fully open level found under control conditions. Under such circumstances only the substate dwell time was fitted to a probability density function. To analyze the concentration and voltage dependence of the occurrence of the QX314-related subconductance state two sorts of measurement were made.

In the first of these, the length of time spent in a given state obtained from the raw lifetime file was used to calculate a measure of the distribution of the open to substate equilibrium. The ratio ($R_{s/o}$) of the total time spent in the QX314-related substate (arrow in the lower right-hand trace in Fig. 7*a*) to the total time spent in the open state (dotted line in the lower right-hand trace in Fig. 7*a*) was determined. An equivalent parameter was also calculated: the fraction (F_s) of total open events occurring as the QX314-related subconductance state—in other words, the total time spent in the substate divided by the total time spent in both the open state and the substate.

In the second method, information was obtained on the kinetics of the interaction of QX314 with the receptor channel by lifetime analysis. Substate and open-state dwell time histograms were compiled with the 50% amplitude threshold method as detailed above. Events of less than 0.18 ms (referred to as t_{min} in Results) could not be fully resolved with low pass filtering at 4 kHz and were removed from the file. Lifetimes were calculated on stripped files containing at least 500 transitions and often more. We followed the methods of Colquhoun and Sigworth (31) in fitting lifetimes to probability density functions. These lifetimes were fitted to probability density functions with one or two exponential terms optimizing the variables to minimize the negative log(likelihood) with a simplex algorithm. A missed-events correction was used as described by Colquhoun and Sigworth (31). The fit to one and two exponential terms was assessed by eye and by using the log(likelihood) ratio test (32); twice the difference in log(likelihood) between the values for one and two exponential terms was tested against a χ^2 distribution at the 1% level with the relevant degrees of freedom. Both open and QX314-related subconductance state lifetime histograms were found to be adequately described by probability density functions with a single exponential term.

RESULTS

The receptor channel is permeable to a wide range of cations and displays a higher conductance with monovalent than with divalent cations (15, 18). Consequently, to maximize the signal-to-noise ratio these experiments were performed in symmetrical 210 mM K^+. Under such conditions the current-voltage relationship is linear, with a slope conductance of approximately 720 pS (Ref. 15 and see Fig. 2).

The objective of this study was to investigate the effects of the "charged" local anesthetics QX222, QX314, and Procaine on cation conductance in the receptor channel. At pH 7.4, QX222 and QX314 are virtually completely ionized, and Procaine is approximately 95% ionized with 5% or so uncharged derivative. No formal study was made of the effect of these compounds on gating. However, qualitatively QX222 and QX314 seemed to be relatively neutral with respect to single-channel open probability (P_o), and Procaine resulted in a time-dependent and reversible decrease.

QX222 and Procaine are voltage-dependent blockers

The addition of millimolar quantities of QX222 or Procaine to the cytoplasmic face of the channel results in a reduction in single-channel current, predominantly at positive holding potentials. The addition of comparable or higher concentrations (for example, up to 10 mM QX222) to the luminal face of the channel results in no measurable effect. Despite this asymmetry of effect, the charged local anesthetics were added symmetrically in order to avoid problems with asymmetric surface potentials developing due to blocker binding to the bilayer on one side of the membrane (33). The effects of the symmetrical addition of 2 mM QX222 and 3 mM Procaine are illustrated in Fig. 1.

The effect of a blocker on single-channel current is dependent on the kinetics of the channel-blocker interaction relative to the filtering and resolution of the recording system. If the kinetics of block are much faster than can be resolved, then block is manifest as a "smooth" time-averaged reduction in single-channel current amplitude (23). Alternatively, if the blocker kinetics are slower and can be resolved, then normal channel openings may be broken up into bursts of much shorter openings representing the entry and exit of blocker in the conduction pathway of the open channel (34). Another possibility is intermediate between the two. The kinetics of blocker interaction may be such that it is manifest as excess noise on the open-channel current amplitude. This is the case with QX222 and Procaine. If the data are filtered at 2 kHz the open channel current amplitude is smeared by noise (see, for example, Figs. 5*a* and 6*a*). However, it is impossible to resolve the individual events even by filtering at 4 kHz. The data were thus filtered at 500 Hz, effectively leading to a smooth block, to measure single-channel current amplitudes (Fig. 1). An example of a single-channel current-voltage relationship in 210 mM K^+ in the absence and in the presence of QX222 is shown in Fig. 2. It is noticeable that in the presence of QX222 there is considerable rectification of the single-channel current at positive holding potentials. A similar phenomenon is observed with Procaine.

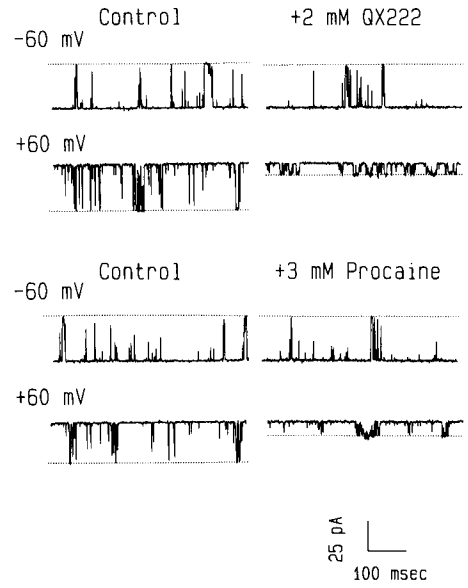

FIGURE 1 Single-channel current fluctuations in symmetrical 210 mM K^+ under the conditions indicated in the figure. The addition of 2 mM QX222 and 3 mM Procaine symmetrically leads to a prominent reduction in single-channel current at positive holding potentials. The traces were filtered at 500 Hz and digitized at 2 kHz. The dotted lines indicate the open channel current level.

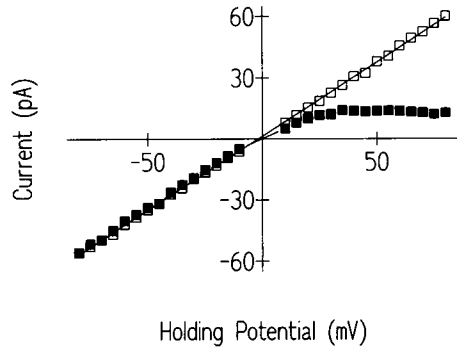

FIGURE 2 A representative single-channel current-voltage relationship in symmetrical 210 mM K^+ (□) and after the addition of 2 mM QX222 (■). The linear regression line through the control points gives a conductance of 726 pS (r = 1.0).

Quantitative analysis of the voltage dependence of block

The standard paradigm for the analysis of voltage-dependent block is due to Woodhull (26). In the simplest form of this analysis there is a single site, accessible to a blocker of valence z from only one side of the channel, lying a fraction δ into the voltage drop. The expression for the change in relative conductance (g/g_o; the current in the presence of blocker divided by the control current) with variations in voltage (V) and blocker concentration ([B]) is

$$\frac{g}{g_0} = \frac{1}{1 + \{[B]/K_b(0)\}e^{z\delta(FV/RT)}} \quad (1)$$

where $K_b(0)$ is the dissociation constant at zero mV holding potential and $z\delta$ is conventionally referred to as the effective valence. F, R, and T have their usual meanings, and RT/F is 25.2 mV at 20°C.

The change in relative conductance with holding potential was measured in 5-mV steps between ±10 and ±80 mV with 2 mM QX222 symmetrically (Fig. 3*a*) and 3 mM Procaine symmetrically (Fig. 3*b*). Eq. 1 was fitted by nonlinear regression to the mean relative conductances (see Materials and Methods). The best-fit parameters for QX222 gave an effective valence of 0.91 ± 0.025 and a zero voltage dissociation constant of 9.2 ± 0.49 mM and for Procaine an effective valence of 0.94 ± 0.028 and a zero voltage dissociation constant of 15.8 ± 0.84 mM (±SEM).

Concentration dependence of QX222 block

The change in relative conductance with varying concentrations of QX222 was investigated at a holding potential of

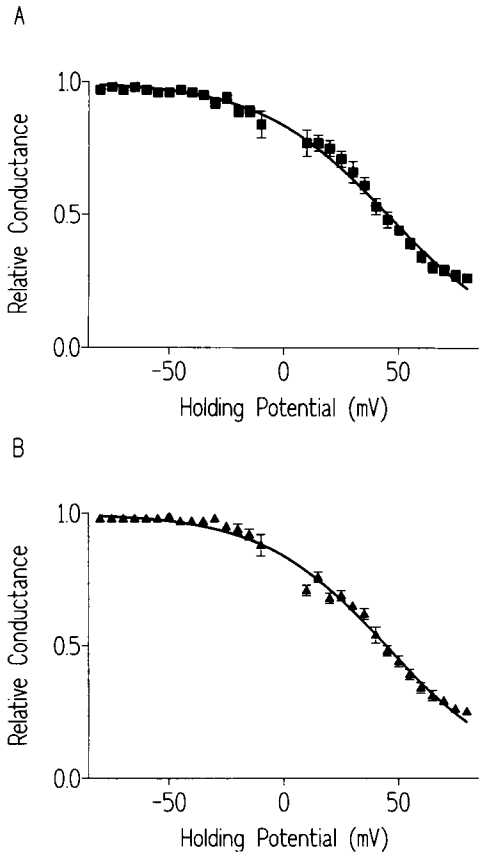

FIGURE 3 (*A*) A plot of mean relative conductance in the presence of 2 mM QX222. The data were obtained from a series of seven experiments, and each point is the mean of at least four observations. Data points are indicated by the squares, with SEM given by the error bars or included within the symbol if smaller. The solid line is the best-fit nonlinear regression line of Eq. 1 with parameters as given in the text. (*B*) A plot of mean relative conductance in the presence of 3 mM Procaine. The data were obtained from a series of five experiments, and each point is the mean of at least four observations. The data points are indicated by the triangles, with SEM given by the error bars or included within the symbol if smaller. The solid line is the best-fit nonlinear regression line of Eq. 1 with parameters as given in the text.

60 mV. The change in relative conductance was described by a simple saturation curve of the type

$$1 - \frac{g}{g_0} = \frac{g_{max} \cdot [B]}{K_m + [B]} \quad (2)$$

where K_m is the concentration at which half-maximal block occurs, g_{max} is the maximal degree of block, and g/g_o and $[B]$ have the same meanings as in Eq. 1.

Fig. 4 shows the mean relative conductances at a series of concentrations. Nonlinear regression (GraphPad Inplot v4. 03) was used to fit Eq. 2 to the data. The best-fit parameters gave a K_m of 491 ± 15 μM and a g_{max} of 0.93 ± 0.01 (±SEM). A Hill plot of the data (not shown) has a slope of 0.84 ± 0.02 (±SEM; r = 0.999). Taken together these data suggest that QX222 interacts with a single site in the conduction pathway and that any positive or negative cooperativity in binding is weak.

Estimating kinetics for QX222 block using amplitude distribution analysis

As explained previously, it is not possible to resolve the individual blocking and unblocking events caused by QX222 and Procaine. However, when filtering at 1–2 kHz these kinetics are manifest as an increase in noise on the open-channel current amplitude. Fitzhugh (27) and Yellen (28) have derived the expected amplitude distribution given first-order filtering of a stochastic transition between the open state and the nonconducting blocked state. In a simplified scheme such as

$$\text{CLOSED} < > \text{OPEN} < > \text{BLOCKED}$$

the filter output of the open to blocked transition is a probability density function of the form

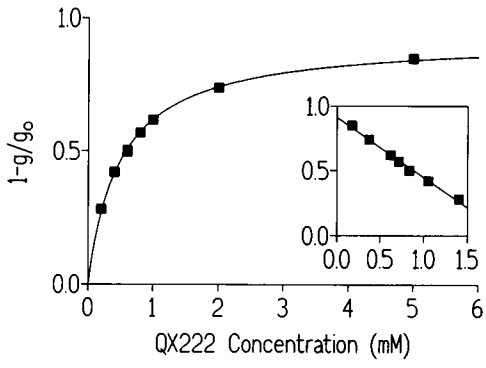

FIGURE 4 A plot illustrating the increase in block, as measured by one minus the relative conductance, at a holding potential of 60 mV with increasing QX222 concentration. The points, as indicated by the squares with SEM contained within the symbol, are the mean of at least four observations from a total of five experiments. The solid line is the best-fit rectangular hyperbola obtained by nonlinear regression with parameters as quoted in the text. The inset is an Eadie-Hofstee plot ($(1 - g/g_o)$ against $(1 - g/g_o)/[QX314]$) of the data with a linear regression line through the points. The slope gives a K_m of 465 μM and a V_{max} of 0.91 (r = –0.997).

$$f(y) = \frac{y^{a-1} \cdot (1-y)^{b-1}}{\int_0^1 y^{a-1} \cdot (1-y)^{b-1}\, dy} \quad (3)$$

where a and b are related to the on (K_{on}) and the off (K_{off}) rate and the filter time constant (τ) by

$$K_{on} = b/\tau \quad (4)$$

and

$$K_{off} = a/\tau \quad (5)$$

These equations only describe an output for a first-order filter. The frequency (f) of the Bessel filter is related to the effective time constant by

$$\tau = \frac{0.228}{f} \quad (6)$$

More details are given in Materials and Methods concerning noise and the fitting of the equation to experimental data. The net result of this approach is that it is possible to derive estimates of K_{on} and K_{off} given the amplitude histogram. We have examined the voltage and concentration dependence of the kinetics of QX222 block using this approach.

The voltage dependence of the kinetics of QX222 block was examined with 500 μM QX222 present symmetrically in 10-mV steps between 40 and 80 mV holding potential. Current amplitudes, in the absence and presence of QX222, were measured in a series of four experiments with 500 Hz filtering. Equation 1 was fitted to the plot of holding potential against mean relative conductance using nonlinear regression; an effective valence of 0.94 ± 0.025 and $K_b(0)$ of 7.9 ± 0.48 mM were calculated (±SEM; data not shown). Thus blocking parameters are similar to those determined at the higher QX222 concentration, as would be expected for a single-site scheme such as the Woodhull model.

Amplitude histograms were then compiled from the data at higher filtering (see Materials and Methods), and Eq. 3, together with convolved and baseline noise, was fitted to the data at a series of holding potentials (Fig. 5*a*). If K_{on} and K_{off} are described by the Boltzmann relationship then

$$K_{on}(V) = K_{on}(0) \cdot e^{z_{on} \cdot (FV/RT)} \quad (7)$$

and

$$K_{off}(V) = K_{off}(0) \cdot e^{-z_{off} \cdot (FV/RT)} \quad (8)$$

where $K(V)$ and $K(0)$ refer to the rate constant at a particular voltage and at 0 mV, respectively. z is the valence of the respective reaction. From a plot of the natural logarithm of the rate constant against holding potential it is possible to determine z from the slope and $K(0)$ from the intercept. The total voltage dependence of the reaction is given by $z_{on} + z_{off}$.

Fig. 5*b* shows such a plot. The voltage dependence lies almost exclusively in K_{on}; the slope corresponds to a valence of 0.92 ± 0.058 (r = 0.994), and the intercept is 1.31 ± 0.143 (corresponding to $K_{on}(0)$ of 3.14 ms^{-1}). K_{off} is probably independent of voltage, and the mean value gives a rate constant of 44.3 ms^{-1}.

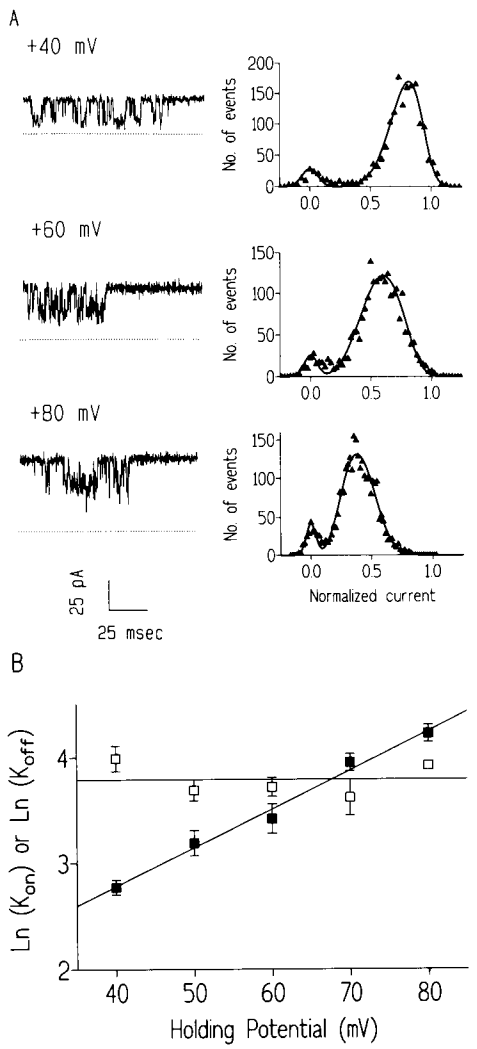

FIGURE 5 (*A*) An illustration of the effect of voltage on single-channel open current amplitude in symmetrical 210 mM K^+ with 500 μM QX222 present at both faces of the channel at a series of holding potentials as indicated in the figure. Short runs of trace are shown beside the amplitude histogram (individual points shown by triangles; compiled and binned as described in Materials and Methods) with the fitted theoretical curve (see text for details). The single-channel current fluctuations at 40 mV were filtered at 1.5 kHz and digitized at 8 kHz, and those at the two higher potentials were filtered at 2 kHz and digitized at 8 kHz. The dotted lines indicate the single-channel current under control conditions in the absence of QX222. The best-fit theoretical function at 40 mV is given by a = 9.38, b = 2.67, baseline noise SD is expressed as a percentage of the control current = 6.6% (σ) and the number of events due to baseline noise n = 134 (n), at 60 mV a = 5.55, b = 3.99, σ = 5.4%, and n = 147, and at 80 mV a = 5.75, b = 8.69, σ = 4%, and n = 246. (*B*) A plot of ln(K_{on}) (■) and ln(K_{off}) (□) against holding potential with 500 μM QX222, which is present symmetrically. The results are the mean of four observations from four experiments. The SEM is indicated by the error bars, except where it is sufficiently small to be within the symbol. The solid lines are derived and have parameters as indicated in the text.

In an analogous manner, it is possible to analyze the concentration dependence of the kinetics for QX222. Amplitude histograms were compiled at 60 mV holding potential at a series of concentrations up to 1 mM, and the composite β function was fitted (Fig. 6*a*). Fig. 6*b* shows the variation of mean K_{on} and K_{off} with QX222 concentration. The major kinetic factor responsible for the increase in block with increasing concentration is a linear variation in K_{on}. Linear regression gives a slope of 0.1 ± 0.003 ms^{-1} μM^{-1} (r = 0.998) and an intercept of −1.36 ± 2.15 ms^{-1}. By contrast, K_{off} is only weakly concentration dependent; if it is assumed to be independent then the mean K_{off} = 52.6 ms^{-1}.

Block by QX314

The effect of QX314 on single-channel current is illustrated in Fig. 7*a*. This effect is present only when QX314 is present

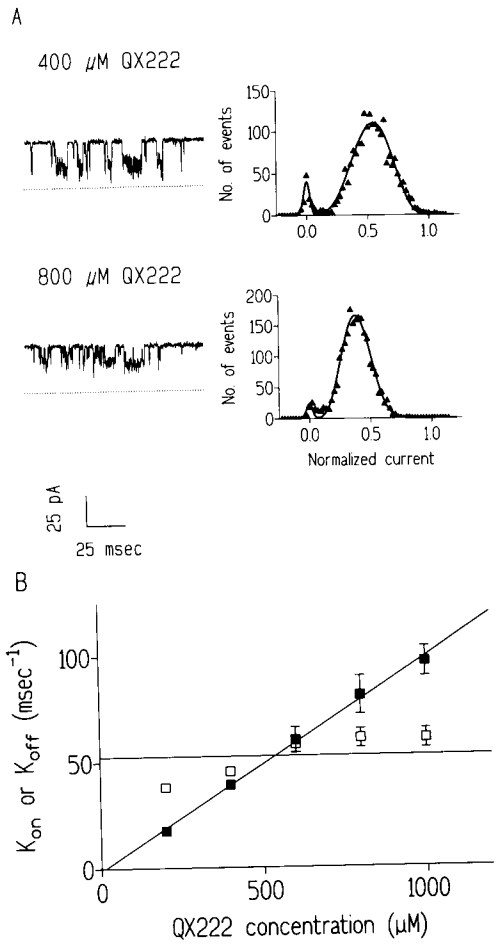

FIGURE 6 (*A*) An illustration of the effect of concentration on single-channel open current amplitude in symmetrical 210 mM K^+ at 60 mV holding potential with varying concentrations of QX222 present at both faces of the channel as indicated in the figure. Short runs of trace are shown beside the amplitude histogram (individual points shown by *triangles*; compiled and binned as described in Materials and Methods) with the fitted theoretical curve (see text for details). The single-channel current fluctuations were filtered at 2 kHz and digitized at 8 kHz. The dotted lines indicate the single-channel current under control conditions in the absence of QX222. The best-fit theoretical function at 400 μM QX222 is given by a = 5.61, b = 4.82, σ = 2.5%, and n = 113, and at 800 μM QX222 a = 7.28, b = 11.3, σ = 2.5%, and n = 69. (*B*) A plot of K_{on} (■) and K_{off} (□) against QX222 concentration at a holding potential of 60 mV. The results are the mean of four observations from four experiments. The SEM is indicated by the error bars except where it is sufficiently small to be within the symbol. The solid lines are derived and have parameters as indicated in the text.

at the cytoplasmic face of the channel and is freely reversed when QX314 is perfused out. The addition of QX314 to the luminal face of the channel has no demonstrable effect. However, to avoid the possibility of asymmetric surface potentials QX314 was added to both chambers in all experiments. Another property of the QX314 substate is shown by Fig. 7 (*b* and *c*); the appearance of the substate is voltage and concentration dependent. In other words as holding potential is made increasingly positive or concentration is increased the proportion of total openings attributable to the substate increases while those attributable to the full open state decrease. The lack of an effect at negative holding potentials in Fig. 7*a* is a manifestation of this voltage dependence.

What proportion of the full amplitude openings is the substate? Fig. 8 shows representative current-voltage relationships. QX314 (300 μM) was present in both chambers, and the substate-related amplitudes were measured only at voltages where it could clearly be identified. From a series of such experiments the substate conductance was measured as 244 ± 15 pS or 0.34 ± 0.02 of the control conductance (n = 6; ±SEM).

Obtaining quantitative information on QX314 block

We have previously described a similar form of block caused by large tetraalkyl ammonium cations (17). Although the technical means of extracting the equilibrium parameters used here is slightly different, the objectives and principles of the analysis are the same. Briefly, these are as follows. Consider the following equilibrium in which a single QX314 binds to the open state to produce the substate

$$\text{CLOSED} < > \text{OPEN} < > \text{SUBSTATE.QX314}$$

If the second equilibrium is voltage dependent then it will be determined by the Boltzmann distribution. The ratio of time spent in the QX314-related substate to that in the fully open state ($R_{s/o}$) will be given by

$$R_{s/o} = e^{[z_t FV - G_i]/RT} \quad (9)$$

where z_t is the total voltage dependence of the effect and G_i/RT is an expression of the equilibrium of the reaction at zero holding potential. Taking the natural logarithm of both sides of Eq. 9 leads to a convenient linearization in which the slope gives the voltage dependence of the open state to substate transitions, and the equilibrium term can be derived from the intercept. In addition, if voltage dependent, K_{on} and K_{off} to and from the substate will be described by equations identical to Eqs. 7 and 8.

Furthermore, this simple scheme predicts that the time spent in the substate expressed as a proportion (F_s) of the total open time (i.e., the time spent in the open state added to time spent in the substate) will show simple saturation with increasing QX314 concentration. Additionally, K_{on} will vary linearly with QX314 concentration and account solely for the equilibrium behavior.

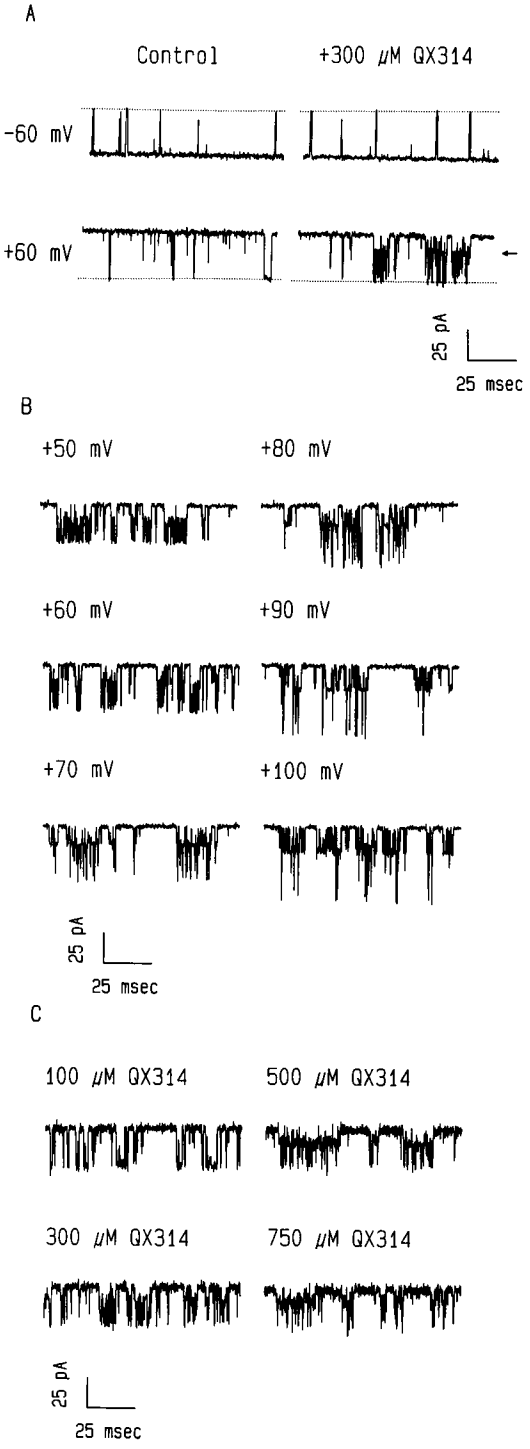

FIGURE 7 (*A*) Representative single-channel current fluctuations under conditions as indicated in the figure. The arrow marks the level of the QX314 related substate apparent at 60 mV holding potential. The data are filtered at 4 kHz and digitized at 10 kHz. The dotted lines indicate the open channel current level. (*B*) The effect of holding potential on single-channel currents in the presence of symmetrical 300 μM QX314. The QX314-related substate becomes increasingly apparent as the holding potential increases. The data are filtered at 4 kHz and digitized at 10 kHz. (*C*) The effect of increasing QX314 concentration on single-channel currents at a holding potential of 60 mV. The QX314-related substate becomes increasingly obvious as the concentration increases. The data are filtered at 4 kHz and digitized at 10 kHz.

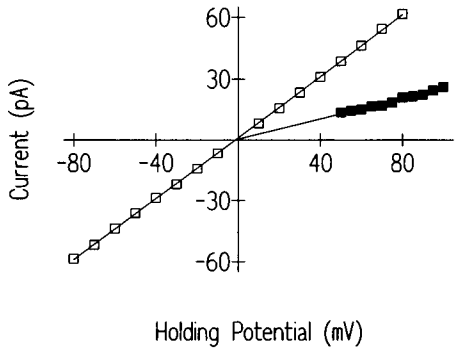

FIGURE 8 A representative current-voltage relationship under control conditions in symmetrical 210 mM K^+ (□) and that for the QX314-related substate (■). The slope conductances derived from the linear regression lines are, respectively, 753 pS (r = 0.99) and 250 pS (r = 0.99).

Equilibrium voltage and concentration dependence of the occurrence of the QX314-related substate

The voltage dependence of the occurrence of the QX314-related substate was investigated with 300 μM QX314 present symmetrically. The behavior of $R_{s/o}$ with varying holding potential was studied at 5-mV steps over the range from 55 to 100 mV. The linearized plot is shown in Fig. 9*a*. This simple formulation describes the behavior well. The slope corresponds to a valence of 1.54 ± 0.055 (r = 0.995), and the intercept is −3.66 ± 0.17 (corresponding to G_i/RT = 0.0273) (±SEM).

The concentration dependence of the occurrence of the QX314-related substate was determined at a holding potential of 60 mV at a series of QX314 concentrations. The behavior of F_s with varying concentration is shown in Fig. 9*b*. Fitted to the data by nonlinear regression is a curve of the type

$$y = 100 \cdot \frac{x^a}{x^a + b^a} \qquad (10)$$

This curve and its linearized equivalent, the Hill plot (shown as an inset in Fig. 9*b*), give a measure of any possible cooperativity in an effect. The slope of the Hill plot and the variable a above are essentially synonymous. The condition $a = 1$ is compatible with binding to a single site, but $a > 1$ suggests positive cooperativity and the value places a lower limit on the number of binding sites. The best-fit parameters to the mean data give a = 1.75 ± 0.084 and b = 239 ± 6.2 μM (± SEM).

Determining kinetics for block by QX314

It is possible to determine kinetics for QX314 block by studying the dwell times in the open state and substate. Both dwell time histograms are adequately described by single exponentials (see Materials and Methods), and examples are shown in Fig. 10. In a simple scheme such as the one above, the reciprocal of the time constant of the single exponential probability density function describing substate dwell times

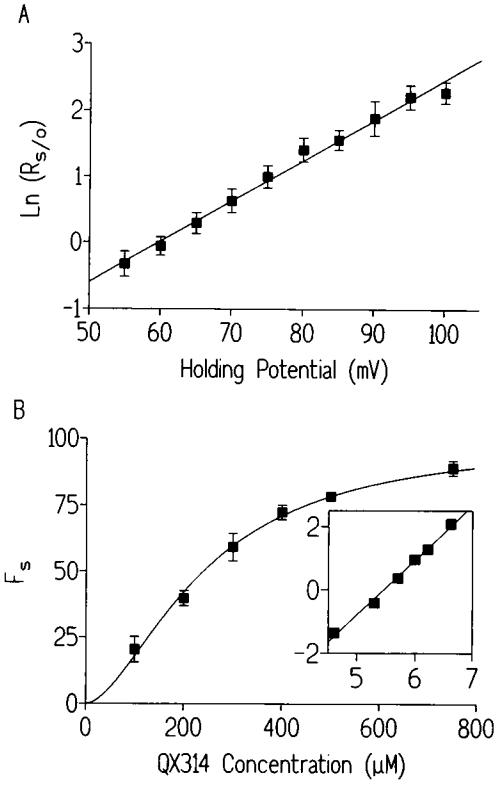

FIGURE 9 (*A*) The variation of ln($R_{s/o}$) with holding potential with 300 μM QX314 present at both faces of the channel. The points indicated by the squares are the mean of at least four observations, except for the 95 mV point, which is based on three observations obtained from five experiments. The SEM on the points is indicated by the error bars. The solid line is a linear regression line with parameters as indicated in the text. (*B*) The variation of F_s with increasing QX314 concentration. The data points indicated by the squares are the mean of at least four observations from seven experiments. The SEM is indicated by the error bars or contained within the symbol. The solid line is the best nonlinear regression fit of Eq. 10 to the data with parameters as given in the text. The inset shows a Hill plot [ln (F_s/(100 − F_s)) against ln([QX314])] of the same data. The slope is 1.73 (r = 0.997).

can be unambiguously interpreted as the QX314 off rate (K_{off}). The interpretation of the open state dwell times is a little more complex. In the simple scheme above there are two ways that an open event can be terminated: by closure or by entry into the substate because of interaction with QX314. The observed rate is a sum of rate constants of the pathways that exit from that state (35, 36). In this case it will be the sum of the on rate for QX314 and the closure rate. The observed rate will reflect K_{on} if the innate rate of closure is much slower than K_{on}. Two pieces of evidence suggest that this may be the case. In the absence of QX314, the open dwell times are described by a probability density function with at least three exponential components (37). In the presence of as little as 100 μM QX314 at holding potentials of 60 mV or more, it is only necessary to use a single exponential term in the probability density function. The second point is that the dwell time reproducibly shortens with increasing QX314 concentration in an approximately linear fashion (see Fig. 11*b*). The reciprocal of the time constant of the single exponential probability density function describing the open-

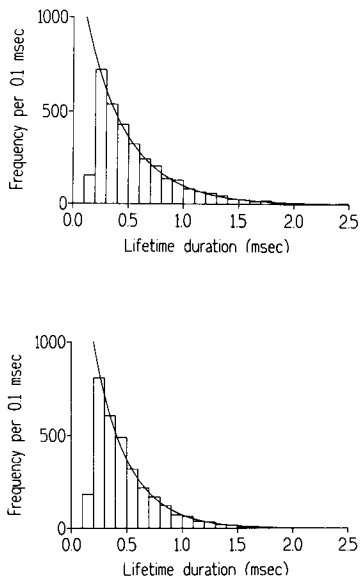

FIGURE 10 The panels show representative lifetime histograms obtained in the presence of symmetrical 300 μM QX314 at a holding potential of 60 mV. The upper panel shows the open lifetime histogram, and the lower panel the substate lifetime histogram together with the superimposed probability density functions (*solid lines*). The data are best described by probability density functions with a single exponential term with τ = 0.376 ms for the open lifetime histogram and τ = 0.302 ms for the substate dwell times.

state dwell times in the presence of QX314 is thus taken as equivalent to K_{on}.

Analyzing the voltage and concentration dependence of the kinetics for QX314

K_{on} and K_{off} were determined at 5-mV steps between 55 and 100 mV holding potential with 300 μM QX314 present symmetrically on both sides of the receptor channel. At and above a holding potential of 85 mV, K_{on} became too fast to measure reliably (i.e., it was difficult to obtain a sufficient number of events above the t_{min} to perform accurate lifetime analysis). K_{off} was determined at all holding potentials. The mean data are shown in Fig. 11*a*. ln(K_{on}) varies linearly with holding potential, as would be expected from Eq. 7, the slope corresponds to a valence of 0.63 $\pm$ 0.015 (r = 0.999), and the intercept is −0.29 $\pm$ 0.037 ($\pm$SEM). The behavior of ln(K_{off}) with increasing holding potential is more complex. It is biphasic in nature—initially decreasing, passing through a minimum, and then increasing. Excluding the points after the minimum it is possible to describe K_{off} between 55 and 85 mV holding potential by Eq. 8. The slope corresponds to a valence of 0.75 $\pm$ 0.039 (r = −0.993) with an intercept of 3.06 $\pm$ 0.109 ($\pm$SEM). Thus, between 55 and 85 mV holding potential the effect would be expected to have a valence of approximately 1.4. This agrees reasonably with the equilibrium measurement based on $R_{s/o}$, although this was determined over the full potential range (over the holding potential range 55 to 85 mV a valence of 1.70 $\pm$ 0.08 is obtained).

In an analogous fashion it is possible to determine the dependence of K_{on} and K_{off} on varying QX314 concentration.

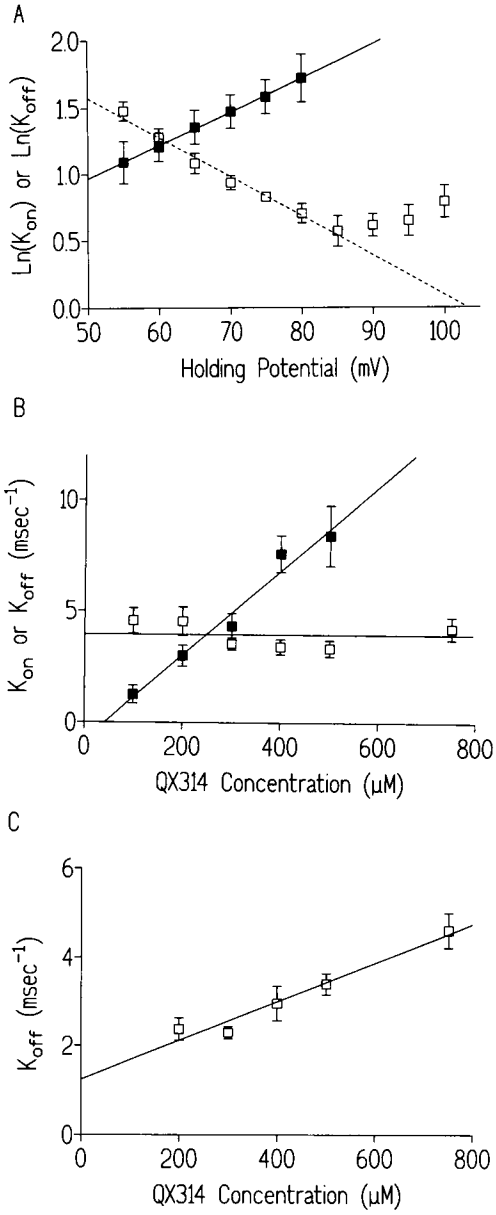

FIGURE 11 (*A*) The variation of ln(K_{on}) (■) and ln(K_{off}) (□) with holding potential. The data were obtained from a series of five experiments, and the data points are the means of at least four observations, except for the point at 95 mV, which is from three observations. The SEM on the points is indicated by the error bars or is within the symbol if smaller. The solid and dashed linear regression lines are calculated and have parameters as described in the text. (*B*) The concentration dependence of K_{on} (■) and K_{off}(□) for QX314 at a holding potential of 60 mV. The points are the mean of at least four observations from seven experiments. The SEM of the points is indicated by the error bars. The solid lines through the points have the theoretical significance and parameters indicated in the text. (*C*) Variation in K_{off} at 80 mV holding potential with increasing QX314 concentration. The points are indicated by the squares from at least four observations from a series of eight experiments. The SEM is indicated by the error bars. The solid line is a linear regression line and has parameters as given in the text.

Fig. 11 shows this at holding potentials of 60 mV (in Fig. 11*b*) and 80 mV (in Fig. 11*c*). At 60 mV holding potential K_{on} was steeply and approximately linearly dependent on concentration; the slope is 0.019 $\pm$ 0.002 $\mu M^{-1}ms^{-1}$ (r = 0.985), and

the intercept is −0.781 ± 0.635 ms^{-1}(±SEM). Above 500 μM QX314 at this holding potential, it is difficult to obtain an accurate measurement of K_{on} because the majority of events are below t_{min}. At this holding potential K_{off} was independent of QX314 concentration. However, intriguingly, this is not the case at 80 mV holding potential (Fig. 11*c*). At this holding potential K_{off} paradoxically increases with increasing concentration in an approximately linear fashion; the slope is 4.37E-3 ± 5.2E-4 $\mu M^{-1}ms^{-1}$ (r = 0.980), and the intercept 1.24 ± 0.24 ms^{-1} (±SEM).

DISCUSSION

The major qualitative observation made in this communication is that the charged local anesthetics reduce K^+ conductance in the sheep cardiac Ca^{2+} release channel in a voltage- and concentration-dependent fashion. The effect occurs only from the cytoplasmic face of the channel. However, the mechanism of block appears to be different for QX222 and Procaine as opposed to QX314. We have previously described two forms of block by tetraalkyl ammonium cations of the receptor channel. The smaller tetraalkyl ammonium cations and related trimethyl ammonium derivatives act as "classical" voltage-dependent blockers (16). The larger members of the group (tetrabutyl and tetrapentyl ammonium cations) cause an unusual form of substate block (17). The charged local anesthetics show some structural similarities to these compounds: in particular, the trimethyl and triethyl ammonium charged groups in QX222 and QX314, respectively, and to a lesser extent the dimethyl ammonium charged group in Procaine.

Procaine and QX222 block

Procaine and QX222 cause a voltage-dependent block with an effective valence of 0.9. In addition, the reduction in single-channel current with increasing QX222 is reasonably approximated by a Langmuir isotherm. A simple way to interpret these findings is that QX222 and Procaine interact with a single site located approximately 90% of the way across the voltage drop of the conduction pathway from the cytoplasmic face of the channel. This agrees with our previous studies in which we found that tetraethyl ammonium (TEA^+), tetrapropyl ammonium, ethyltrimethyl ammonium, and propyltrimethyl ammonium cations have a similar effective valence and that TEA^+ appears to interact at a single site. It seems likely that the charged local anesthetics and the aforementioned small tetraalkyl ammonium cations interact at the same position in the conduction pathway.

In addition, the use of amplitude distribution analysis has revealed that the QX222 on rate almost solely accounts for the concentration and voltage dependence of the blocking reaction. The strong and almost exclusive voltage dependence of K_{on} has been noted with block in other channels (e.g., by bis Qx_n in the SR K^+ channel) (33). Interpreting this observation in terms of a rate theory description implies asymmetry of the energy profile for the blocker. A highly negatively charged binding site may screen or complex with QX222. This could effectively reduce or abolish the charge in the unblocking transition complex; K_{off} may then be less voltage dependent than K_{on} as a result (38).

The linear increase of K_{on} with increasing concentration is as expected for an interaction with a single site. However, K_{off} does appear to be slightly concentration dependent. The Hill plot for the reduction in single-channel current with increasing QX222 concentration is 0.84. These deviations are relatively small; the fit of a rectangular hyperbola to the data and the straight line to the Eadie-Hofstee plot in Fig. 4 look close, and K_{on} is 3 to 4 times more concentration dependent than K_{off}. One alternative is that QX222 is acting at two sites within the conduction pathway, each with a different affinity and voltage dependence, to block single-channel current. However, the observation that the voltage dependence of block is almost identical at 0.5 and 2 mM QX222 argues against this interpretation. Another explanation could involve the presence of significant negative charge on the surface of the protein surrounding the conduction pathway; increasing concentrations of blocker would screen this charge. This explanation has been invoked to explain a much more significant deviation found with Ca^{2+} block in voltage-dependent sodium channels (39). The ionic conditions and the monovalent nature of the blocker used in these experiments would lead to a quantitatively smaller effect, but at mM concentrations of QX222 this may lead to a minor but statistically measurable effect. Unfortunately our efforts to provide independent evidence for and measurement of surface charge on the protein have been hindered by the absence of an inert cation.

Our failure to observe a consistent and reproducible increase in P_o and open times in the presence of and with increasing concentrations of blocker argues against a simple closed open blocked scheme and suggests, for example, that the blocker may be able to bind to and unbind from the closed channel. An alternative explanation may be advanced from recent work (40) on the effects of the local anesthetics on the purified skeletal SR Ca^{2+} release channel reconstituted into planar phospholipid bilayers. These authors propose the existence of two binding sites for local anesthetics on the skeletal SR Ca^{2+} release channel: a relatively low affinity blocking site within the conduction pathway and another site, external to the conduction pathway, the occupancy of which leads to a decline in single-channel P_o. For any particular anesthetic there may thus be two opposing influences combining to affect single-channel P_o.

A minimal kinetic scheme for QX314 block

QX314 presents an unusual and distinctive kinetic picture unlike that seen with Procaine and QX222. The addition of QX314 leads to the voltage- and concentration-dependent appearance of a substate with an amplitude that is one-third that of the control current. Quantitative measurements of the voltage dependence give a valence for the effect of approximately 1.45. The concentration dependence demands that at

least two molecules of QX314 bind to the single channel. These kinetic arguments have the consequence that if QX314 enters the conduction pathway then at least two molecules must do so to generate the kinetic behavior.

However, the substate dwell times have some additional properties. Dwell times are biphasic in nature (Fig. 11*a*) with a maximum at 85 mV. Additionally, if K_{off} is measured at 80 mV holding potential it increases linearly with QX314 concentration above 300 μM. The implication is that the shortening of substate dwell time is dependent on QX314 concentration and voltage. One possible kinetic scheme is

$$\text{OPEN} \underset{k_{-1}}{\overset{k_1}{<>}} \text{QX314.SUBSTATE} \underset{k_{-2}}{\overset{k_2}{<>}} \text{QX314}_2\text{.SUBSTATE} \underset{k_{-3}}{\overset{k_3}{<>}} \text{QX314}_3\text{.BLOCKED}$$

Three molecules of QX314 are assumed to bind—one to the open state and two to the substate. The total voltage dependence of substate appearance should be approximately 1.5, equally resident in K_{on} and K_{off}, and the scheme must include a second lower-affinity QX314 concentration-dependent process that can shorten the substate dwell time (in other words, a substate closed/blocked transition). This process is sufficiently voltage dependent so that it can not only nullify the natural tendency for dwell times to lengthen, but at high enough holding potentials it can cause them to shorten. Such criteria will be met if the three rate constants k_1, k_2, and k_3 were assumed to be concentration and voltage dependent, with a single QX314 traversing 75% of the voltage drop to produce the substate and 90% of the voltage drop to completely occlude the substate. The unbinding rates are assumed to be invariant with voltage and concentration. In this scheme the open times will be described by a probability density function with a single exponential term, but the substate dwell times ought to be described, at least theoretically, by a probability density function with two exponential terms. However, if one of the transitions is fast enough to be below the time resolution of the system or forms a very small proportion of the observed probability density function, only one time constant may be apparent. Quantitative modeling (not shown) based on such a scheme is able to reproduce qualitatively the biphasic nature of the voltage dependence, the paradoxical increase of K_{off} with increasing concentration at 80 mV, and the failure to observe a similar effect at 60 mV holding potential. It is difficult, however, to fit quantitatively all of the data despite many variations of rate constants. The model is able to predict accurately the equilibrium behavior of the substate appearance.

It has been taken as read that the two forms of block, "classical" block as manifest by QX222 on the one hand and "substate" block, for example, as caused by QX314 on the other, are different and distinct phenomena. Despite the differences in apparent affinity and voltage dependence is it possible that the time-averaged reduction in relative conductance seen with the smooth blockers involves the transition to a substate followed by a subsequent transition to a fully blocked state of zero conductance? It is not possible to directly observe transitions to the closed state with those members of the first group such as QX222. However, the modeling work suggests that if block were time-averaged, then for both the voltage and concentration dependence two components to the smooth block would be detected.

Physical interpretations of block

The occurrence of "substate block" is being increasingly reported in a variety of channels. In the proton-dependent effect in the dihydropyridine receptor (41, 42), the zinc effect in the cardiac batrachotoxin-modified voltage-activated sodium channel (39, 43), and the bovine pancreatic trypsin inhibitor effect in the large conductance Ca^{2+}-activated K^+ channel (44, 45) the conductance change was represented by an allosteric model in which there is a conformational equilibrium between the open state and substate levels, a transition highly favored in the presence of blocker.

The alternative hypothesis is that the interacting species directly enter the conduction pathway to cause a form of partial block. We have used such an explanation (17) to account for the production of substates by tetrabutyl (TBA^+) and tetrapentyl ammonium ($TPeA^+$) cations. The existence of yet a third substate level (the levels with TBA^+ and $TPeA^+$ were 21% and 14% of the control current, respectively) and some kinetic differences argue against a common kinetic scheme responsible for all of these different forms of substate block. However, it seems more likely that the different substates and the kinetics of their production are explained by the physical characteristics of the blocker inducing them and its interaction with the receptor channel conduction pathway.

It is possible that the transition from substate to blocked state with QX314 is a manifestation of block similar in type to that seen with QX222. The data and minimal kinetic scheme for QX314 are compatible with the proposition that the three charged local anesthetics are able to bind to a single site in the constricted portion of the channel 90% across the voltage drop to completely occlude current flow. QX314 has the additional property that it is able to induce a substate.

The model (not shown), although successful qualitatively, is not so quantitatively accurate for certain kinetic aspects. Excluding transitions to the blocked state and assuming that QX314 interacts only with the open state, the minimal kinetic scheme proposed for QX314 block is a subset of the general sequential scheme

$$\text{OPEN} <> \cdots <> [\text{QX314}]_{X-1}\text{OPEN} <> [\text{QX314}]_X\text{SUBSTATE} <> \cdots <> [QX314]_Y\text{SUBSTATE}$$

where X cations bind to the open state to produce the substate and Y can bind to the substate. This general scheme for sub-

state block in the Ca^{2+} release channel would allow us to incorporate our previous observations of substate block by TBA^+ and $TPeA^+$. The kinetic variability apparent between QX314, TBA^+, and $TPeA^+$ could be explained by variations in x and y and the interaction of the blocker with the binding sites. For example, the possibility of binding several QX314s means that each need only traverse a fraction of the voltage drop but still cause a highly voltage-dependent effect, and several QX314s binding to the substate leads to highly voltage-dependent off rates.

Given this kind of general kinetic scheme, how might the occurrence of substates be explained in physical terms? It is becoming increasingly apparent from biophysical and cloning studies that the conduction pathways of biological ion channels consist of vestibules of varying sizes either side of a constriction. If the SR Ca^{2+} release channel had a relatively large vestibule facing the cytoplasm, this could act as a binding site for the blockers and interaction here would produce partial but not complete occlusion. Theoretical calculations have been carried out that suggest that a significant proportion of the voltage drop may fall over such a wide vestibule, and thus binding and unbinding could be voltage dependent (46). Modeling studies have been carried out to examine the influence of vestibule charge and dimensions on ion conduction (47, 48). In particular, it is possible to generate substates by two major electrostatic means: minor changes in the structure of the vestibule, such as may occur on the binding of the blocker, alter the way in which the electric field distributes itself across the vestibule, and the binding of cations to negative vestibule charge can reduce the ability of the vestibule to concentrate ions (48). A further nonelectrostatic factor may be the reduction in channel capture radius consequent upon blocker binding (45).

Physiological significance of local anesthetic block

The observations made in this paper detail two mechanisms by which Ca^{2+} release from the SR may be inhibited by charged local anesthetics. The concentration of Procaine inhibiting Ca^{2+} efflux from SR vesicles by 50% was 2.1 mM (22), and this is in the kind of low mM range we observe for the $K_b(0)$ for QX222 and Procaine. In addition, those experiments were carried out at lower ionic strength. While it is difficult to reliably equate two such different techniques, the quantitative data do suggest that channel blockade may be a component in the inhibition of Ca^{2+} release from the SR.

There is increasing interest in cytosolic Ca^{2+} oscillations in cardiac cells in pathologic conditions, in particular the possibility of such changes leading to cardiac arrhythmogenesis. It is thought possible that such oscillations are reflected in variations in a transient inward current i_{ti} at the cell membrane, carried most probably by the Na^+-Ca^{2+} exchange (49, 50). The proposition is that these events in turn are dependent on SR calcium release. The ability to block this release under such abnormal circumstances then assumes much greater importance. An understanding of the factors and mechanisms involved in block of the Ca^{2+} release channel of cardiac SR may have practical significance in leading to possible strategies designed to prevent and treat cardiac arrhythmias.

We would like to thank Dr. Allan Lindsay for his help in the preparation of the purified Ca^{2+} release channel and with elements of the computing. We are grateful to Astra Pharmaceuticals for the generous gifts of QX222 and QX314.

This work was supported by the Medical Research Council and the British Heart Foundation.

REFERENCES

1. Fabiato, A. 1989. Appraisal of the physiological relevance of two hypotheses for the mechanism of calcium release from the mammalian cardiac sarcoplasmic reticulum: calcium-induced release versus charge-coupled release. *Mol. Cell. Biochem.* 89:135–140.
2. Wier, W. G. 1990. Cytoplasmic [Ca^{2+}] in mammalian ventricle: dynamic control by cellular processes. *Annu. Rev. Physiol.* 52:467–485.
3. Rios, E., J. J. Ma, and A. Gonzalez. 1991. The mechanical hypothesis of excitation-contraction (EC) coupling in skeletal muscle. *J. Muscle Res. Cell Motil.* 12:127–135.
4. Miyamoto, H., and E. Racker. 1982. Mechanism of calcium release from skeletal muscle sarcoplasmic reticulum. *J. Membr. Biol.* 66:193–201.
5. Smith, J. S., R. Coronado, and G. Meissner. 1985. Sarcoplasmic reticulum contains adenine nucleotide-activated calcium channels. *Nature (Lond.)* 316:446–449.
6. Rousseau, E., J. S. Smith, J. S. Henderson, and G. Meissner. 1986. Single channel and $^{45}Ca^{2+}$ flux measurements of the cardiac sarcoplasmic reticulum calcium channel. *Biophys. J.* 50:1009–1014.
7. Holmberg, S. R. M., and A. J. Williams. 1989. Single channel recordings from human cardiac sarcoplasmic reticulum. *Circ. Res.* 65:1445–1449.
8. Smith, J. S., R. Coronado, and G. Meissner. 1986. Single channel measurements of the calcium release channel from skeletal muscle sarcoplasmic reticulum. *J. Gen. Physiol.* 88:573–588.
9. Ashley, R. H., and A. J. Williams. 1990. Divalent cation activation and inhibition of single calcium release channels from sheep cardiac sarcoplasmic reticulum. *J. Gen. Physiol.* 95:981–1005.
10. Williams, A. J. 1992. Ion conduction and discrimination in the sarcoplasmic reticulum ryanodine receptor/calcium-release channel. *J. Muscle Res. Cell Motil.* 13:7–26.
11. Inui, M., A. Saito, and S. Fleischer. 1987. Purification of the ryanodine receptor and identity with feet structures of junctional terminal cisternae of sarcoplasmic reticulum from fast skeletal muscle. *J. Biol. Chem.* 262:1740–1747.
12. Inui, M., A. Saito, and S. Fleischer. 1987. Isolation of the ryanodine receptor from cardiac sarcoplasmic reticulum and identity with the feet structures. *J. Biol. Chem.* 262:15637–15642.
13. Lai, F. A., H. P. Erickson, E. Rousseau, Q-Y. Liu, and G. Meissner. 1988. Purification and reconstitution of the Ca release channel from skeletal muscle. *Nature (Lond.)* 331:315–319.
14. Lindsay, A. R. G., and A. J. Williams. 1991. Functional characterisation of the ryanodine receptor purified from sheep cardiac muscle sarcoplasmic reticulum. *Biochim. Biophys. Acta* 1064:89–102.
15. Lindsay, A. R. G., S. D. Manning, and A. J. Williams. 1991. Monovalent cation conductance in the ryanodine receptor-channel of sheep cardiac muscle sarcoplasmic reticulum. *J. Physiol.* 439:463–480.
16. Tinker, A., A. R. G. Lindsay, and A. J. Williams. 1992. Block of the sheep cardiac sarcoplasmic reticulum Ca^{2+}-release channel by tetraalkyl ammonium cations. *J. Membr. Biol.* 127:149–159.
17. Tinker, A., A. R. G. Lindsay, and A. J. Williams. 1992. Large tetraalkyl ammonium cations produce a reduced conductance state in the sheep cardiac sarcoplasmic reticulum Ca^{2+}-release channel. *Biophys. J.* 61: 1122–1132.
18. Tinker, A., and A. J. Williams. 1992. Divalent cation conduction in the ryanodine receptor-channel of sheep cardiac muscle sarcoplasmic reticulum. *J. Gen. Physiol.* 100:479–493.

19. Tinker, A., A. R. G. Lindsay, and A. J. Williams. 1992. A model for ionic conduction in the ryanodine receptor-channel of sheep cardiac muscle sarcoplasmic reticulum. *J. Gen. Physiol.* 100:495–517.
20. Endo, M. 1977. Calcium release from the sarcoplasmic reticulum. *Physiol. Rev.* 57:71–108.
21. Chamberlain, B. K., P. Volpe, and S. Fleischer. 1984. Calcium-induced calcium release from purified cardiac sarcoplasmic reticulum vesicles. General characteristics. *J. Biol. Chem.* 259:7540–7546.
22. Chamberlain, B. K., P. Volpe, and S. Fleischer. 1984. Inhibition of calcium-induced calcium release from purified cardiac sarcoplasmic reticulum vesicles. *J. Biol. Chem.* 259:7547–7553.
23. Hille, B. 1984. Ionic Channels of Excitable Membranes. Sinauer, Sunderland, MA.
24. Hille, B. 1977. The pH-dependent rate of action of local anesthetics on the node of Ranvier. *J. Gen. Physiol.* 69:475–496.
25. Miller, C. 1982. Open-state substructure of single chloride channels from Torpedo electroplax. *Philos. Trans. R. Soc. Lond. B Biol. Sci.* 299:401–411.
26. Woodhull, A. M. 1973. Ionic blockage of sodium channels in nerve. *J. Gen. Physiol.* 61:687–708.
27. Fitzhugh, R. 1983. Statistical properties of the asymmetric random telegraph signal, with application to single-channel analysis. *Math. Biosci.* 64:75–89.
28. Yellen, G. 1984. Ionic permeation and blockade in Ca^{2+}-activated K^+ channels of bovine chromaffin cells. *J. Gen. Physiol.* 84:157–186.
29. Quayle, J. M., N. B. Standen, and P. R. Stanfield. 1988. The voltage-dependent block of ATP-sensitive potassium channels of frog skeletal muscle by caesium and barium ions. *J. Physiol.* 405:677–698.
30. Press, W. H., B. P. Flannery, S. A. Teukolsky, and W. T. Vetterling. 1989. Numerical Recipes in Pascal. Cambridge University Press, Cambridge.
31. Colquhoun, D., and F. J. Sigworth. 1983. Fitting and statistical analysis of single-channel recording. *In* Single-Channel Recording. B. Sakmann and E. Neher, editors. Plenum, New York and London. 191–263.
32. Blatz, A. L., and K. L. Magleby. 1986. A quantitative description of 3 modes of activity of fast chloride channels from rat skeletal muscle. *J. Physiol.* 378:141–174.
33. Miller, C. 1982. Bis-Quaternary ammonium blockers as structural probes of the sarcoplasmic reticulum K^+ channel. *J. Gen. Physiol.* 79: 869–891.
34. Neher, E., and J. H. Steinbach. 1978. Local anaesthetics transiently block currents through single acetylcholine-receptor channels. *J. Physiol.* 277:153–176.
35. Colquhoun, D., and A. G. Hawkes. 1977. Relaxation and fluctuations of membrane currents that flow through drug-operated channels. *Proc. R. Soc. Lond. B Biol. Sci.* 199:231–262.
36. Colquhoun, D., and A. G. Hawkes. 1982. On the stochastic properties of bursts of single ion channel openings and clusters of bursts. *Phil. Trans. R. Soc. Lond. B Biol. Sci.* 300:1–59.
37. Sitsapesan, R., A. R. G. Lindsay, and A. J. Williams. 1992. Ca^{2+} activation of the Ca^{2+}-release/ryanodine receptor channel purified from cardiac sarcoplasmic reticulum. *Biophys. J.* 61:A432, 2486. (Abstr.)
38. Moczydlowski, E. 1986. Single-channel enzymology. *In* Ion Channel Reconstitution. C. Miller, editor. Plenum Press, New York and London. 75–113.
39. Ravindran, A., L. Schild, and E. Moczydlowski. 1991. Divalent cation selectivity for external block of voltage-dependent Na^+ channels prolonged by batrachotoxin. Zn^{2+} induces discrete substates in cardiac Na^+ channels. *J. Gen. Physiol.* 97:89–115.
40. Xu, L., R. Jones, and G. Meissner. 1993. Effects of local anesthetics on single channel behavior of skeletal muscle calcium release channel. *J. Gen. Physiol.* 101:207–233.
41. Prod'hom, B., D. Pietrobon, and P. Hess. 1987. Direct measurement of proton transfer rates to a group controlling the dihydropyridine-sensitive Ca^{2+} channel. *Nature (Lond.)* 329:243–246.
42. Pietrobon, D., B. Prod'hom, and P. Hess. 1989. Interactions of protons with single open L-type calcium channels. pH dependence of proton-induced current fluctuations with Cs^+, K^+ and Na^+ as permeant ions. *J. Gen. Physiol.* 94:1–21.
43. Schild, L., A. Ravindran, and E. Moczydlowski. 1991. Zn^{2+}-induced subconductance events in cardiac Na^+ channels prolonged by batrachotoxin. Current-voltage behavior and single-channel kinetics. *J. Gen. Physiol.* 97:117–142.
44. Lucchesi, K. J., and E. Moczydlowski. 1991. On the interaction of bovine pancreatic trypsin inhibitor with maxi Ca^{2+}-activated K^+ channels. A model system for analysis of peptide-induced subconductance states. *J. Gen. Physiol.* 97:1295–1319.
45. Moczydlowski, E., G. W. J. Moss, and K. J. Lucchesi. 1992. Bovine pancreatic trypsin inhibitor as a probe of large conductance Ca^{2+}-activated K^+ channels at an internal site of interaction. *Biochem. Pharmacol.* 43:21–28.
46. Jordan, P. C. 1986. Ion channel electrostatics and the shapes of channel proteins. *In* Ion Channel Reconstitution. C. Miller, editor. Plenum Press, New York and London. 37–55.
47. Dani, J. A. 1986. Ion-channel entrances influence permeation. Net charge, size, shape and binding considerations. *Biophys. J.* 49:607–618.
48. Dani, J. A., and J. A. Fox. 1991. Examination of subconductance levels arising from a single ion channel. *J. Theor. Biol.* 153:401–423.
49. Noble, D. 1984. The surprising heart: a review of recent progress in cardiac electrophysiology. *J. Physiol.* 353:1–50.
50. January, C. T., and H. A. Fozzard. 1988. Delayed after depolarizations in heart muscle: mechanisms and relevance. *Pharmacol. Rev.* 40: 219–227.